

pubs.acs.org/acsapm Article

# Biobased Semi-Interpenetrating Polymer Networks of Poly(*E*-caprolactone) and Epoxidized Soybean Oil with Nanoscale Morphology, Shape-Memory Effect, and Biocompatibility

Samy A. Madbouly,\* Setsuko Yamane, André J. van der Vlies, and Urara Hasegawa



Cite This: https://doi.org/10.1021/acsapm.3c01270

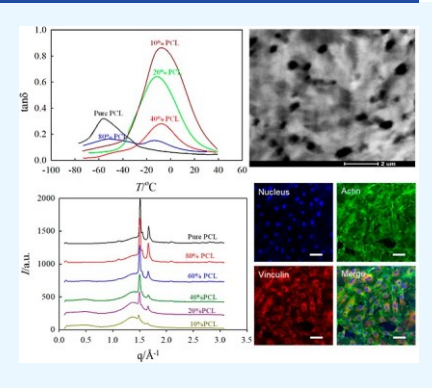


**ACCESS** 

Metrics & More

Article Recommendations

ABSTRACT: Creating biobased polymer blends with outstanding properties, nanoscale morphology, shape-memory capability, and biocompatibility is very crucial and requires a fundamental understanding of the phase behavior, macromolecular structure, and biological compatibility of the polymer blends with living cells. It is very critical to understand the complex relationships among the polymer structure, morphology, and performance of multifunctional smart materials under conditions that they are likely to encounter during use, particularly in biomedical applications. Biobased semi-interpenetrating polymer networks of poly( $\varepsilon$ -caprolactone) and epoxidized soybean oil with nanoscale morphology have been successfully synthesized via in situ cationic polymerization and compatibilization in a homogeneous solution. Varies analytical and characterization techniques, such as Fourier transform infrared spectroscopy, differential scanning calorimetry, dynamic mechanical analysis, transmission electron microscopy, X-ray scattering, cell toxicity, and shape-memory effects (SMEs), have been employed to



understand the structure–properties relationship of these smart, biobased nanostructured polymer blends. The synthesized nano blends were nontoxic or biocompatible and supported attachment of human vein endothelial cells, showing their potential use in biomedical applications. The current versatile, low-cost strategy for synthesizing the nanoscale morphology of semi-interpenetrating polymer networks with SMEs and biocompatibility should be widely applicable for polymer systems. This study is also considered as a continuation to our efforts in the area of biobased polymers to develop innovative technologies to transform natural resources into smart multifunctional materials for a wide range of applications, including coatings, adhesives, and medical devices.

KEYWORDS: semi-interpenetrating network, polymer blends, nanomorphology, biobased polymers, biocompatibility

# INTRODUCTION

Petroleum-based thermoplastics and thermosetting polymers are widely used in many industrial applications including automotive, aerospace, marine, medical, packaging, oil/gas, construction, and many others due to their excellent mechanical, electrical, and thermal properties as well as easy processability and low cost. Regardless of the above-mentioned advantages, the majority of petroleum-based polymers are synthesized from nonrenewable and nondegradable resources with some exceptions such as poly( $\varepsilon$ -caprolactone) (PCL) and poly(butylene succinate). For this reason, production and applications of petroleum-based polymers might lead to a high risk for air, water, and soil pollution. In addition, petroleumbased products are not sustainable and have fluctuated in price due to unexpected political and economic factors. Therefore, biobased and biodegradable polymers with outstanding mechanical, thermal, chemical, and biological properties were recently developed as alternatives to petroleum-based counterparts. There are many cost-effective sustainable environmentally friendly feedstocks or biomasses that can be utilized to produce biobased polymers and composites.<sup>1-7</sup> Wood,

lignocellulose, starch, sugar, proteins, and plant oils are the most widely used renewable feedstocks in making different biobased polymers for different industrial applications. Plant oils are readily available and cost-effective materials in a large volume.<sup>8–15</sup> The chemical structures of all plant oils contain triglycerides of fatty acids of different degrees of unsaturation (i.e., the number of carbon–carbon double bonds). Plant oils can be chemically modified and functionalized into different reactive functional groups, such as hydroxyl, carboxylic acid, epoxy, amines, etc., to increase their utilization in making sustainable products.<sup>16–25</sup> Based on the different chemical modifications and functionalizations, plant oils can be used to

Received: June 14, 2023 Revised: October 2, 2023 Accepted: October 9, 2023



synthesize many biobased polymers including polyesters, polyurethanes, and polyamides.<sup>26–31</sup>

Soybean is the second largest crop plant in the United States. Soybean oil contains different fatty acids, including 53% linoleic, 25% oleic, 10% palmitic, 5% stearic, and 7% linolenic.<sup>32,33</sup> Epoxidized soybean oil (ESO) can be obtained from the epoxidation process of soybean oil by adding an oxygen atom (peroxide or peracid/peroxy acid) to convert the -C□C- bond into an epoxide group.<sup>34</sup> The ESO is commonly used as a green plasticizer in the manufacturing of PVC plastics.<sup>35,36</sup> The epoxy groups in ESO are also more reactive than the −C□C− bond, allowing facile modifications. The chemically modified soybean oil with hydroxyl groups is commonly used for polyurethane synthesis. ESO was also previously incorporated into ionic polymer surfactants that were commonly used in paints, coatings, medicine, and many other applications. 20,37-39 Furthermore, anionic polymers based on ESO were employed as an effective carrier for anticancer drug doxorubicin hydrochloride (Dox) to enhance Dox toxicity against multidrug-resistant cancer cells.<sup>40</sup>

Ring-opening polymerization of the epoxide groups of ESO can be carried out using boron trifluoride diethyl etherate (BF<sub>3</sub>·OEt<sub>2</sub>) as a catalyst in a homogeneous solution of methylene chloride. 41 The obtained ESO polymer cannot be recycled or reprocessed because it is a thermoset polymer. Intarabumrung et al. successfully synthesized a biobased polyamide from ESO and hexamethylene diamine at a high temperature with no solvent or catalyst. 42 The ESO-based polyamide was found to have outstanding electrical performance compared to other biobased polymers due to the significant numbers of nitrogen atoms within the polyamide structure. The ESO-based polyamide could be utilized in manufacturing triboelectric nanogenerators as a sustainable energy-harvesting device. The material was found to be biodegradable in soil, and the biodegradation rate reached up to 17.7 wt % in soil after 28 days. Biobased polyacrylateepoxidized soybean oil (poly-AESO) with a modified ethyl cellulose macromonomer (ECM) was recently processed using 3-D printing technique by Liu et al.<sup>43</sup> A layer-by-layer deposition process followed by rapid UV curing was carried out during the 3-D printing process. A considerable improvement in the mechanical properties of poly-AESO, particularly strength and stiffness, was observed by adding ECM. The glass-transition temperature ( $T_g$ ) of ECM-AESO increased systematically with increasing ECM content.<sup>43</sup> For example, the  $T_{\rm g}$  increased from 47 °C for the pure poly-AESO thermoset to 82 °C for ECM-AESO copolymers with 30 wt % ECM. They also showed that the mechanical and physical properties of ECM-AESO copolymer thermosets can be modulated by changing the content and molecular weight of ECM as well as by various degrees of acrylate substitution. The pure AESO has unsaturated -C C, which can be polymerized or copolymerized via free radical polymerization using different initiators such as UV, high-energy radiation, and photo initiators. The poly-AESO thermoset was used in coating applications due to its good thermal stability. However, the mechanical properties of the poly-AESO thermoset are very poor. To overcome this limitation, the composites of the poly-AESO thermoset with different fibers, such as carbon and glass fibers as well as natural fillers, have been developed. 44-46 Polyols based on ESO and glycerin were employed to synthesize biobased polyurethane thermosets.<sup>47</sup> The curing kinetics was investigated as a function of isocyanate index,

catalyst, and cross-linker concentration. The  $T_g$  of the fully cured sample was approximately 200 °C as determined from the temperature of the peak maximum of tan  $\delta$  (dynamic mechanical analysis, DMA). The flexural modulus and flexural strength of the fully cured sample were about 2.14 and 99.4 GPa, respectively. The curing kinetics of the polyurethane thermoset was evaluated by using the autocatalytic heat flow model, where the vitrification process was preponderant in the evolution of conversion. A recyclable biobased adhesive based on ESO and the dithiol borate ester (BDB) curing agent with excellent adhesion properties (adhesion strength from 3.84 to 9.61 MPa) on different substrates, such as wood, glass, metal, and bamboo plates, has been recently developed by Li et al. 48 The sulfhydryl groups of BDB and the epoxy groups of ESO produced significant numbers of hydroxyl groups that used to make strong hydrogen bonds with the different substrates and consequently developed very high adhesion strength. The recyclability of this adhesive was attributed to the borate ester bonds and their dynamic for topological rearrangement at the evaluated temperature. The ESO-based adhesives showed excellent thermal stability and a high tensile strength up to 25 MPa. Acar et al. synthesized a cold water-soluble, soy oil-based polymer via autoxidation process in air under daylight at room temperature. 49 The molecular weight of the soy oil polymer obtained from this oxidation process was found to be a function of the oxidation time and thickness of soy oil at the beginning of the reaction. The obtained soy oil polymer was then reacted with a diethanol amine to synthesize a cold watersoluble hydroxylated soya oil polymer. The obtained polymers were characterized with several techniques including FTIR, elemental analysis, <sup>13</sup>C NMR, and rheology. <sup>49</sup>

PCL is a petroleum-based semicrystalline polyester synthesized via the ring-opening polymerization of  $\varepsilon$ -caprolactone. The PCL has a  $T_g$  of approximately -60 °C and a melting temperature of about 60 °C. It is also a biodegradable, biocompatible, and bioresorbable polymer. Therefore, PCL has been widely used in many biomedical\_applications including drug delivery and tissue engineering. A composite based on a PCL matrix containing carbon nanotubes (CNTs) and hydroxyapatite (HA) as reinforcement fillers has recently been developed for fabrication of hard tissue scaffolds using selective laser sintering by Feng et al.53 The dispersion of CNT and HA fillers was significantly improved via hydrothermal reaction, where the HA nanoparticles were in situ synthesized on the surface of carboxyl multiwalled CNTs to prevent their aggregation. Shape-memory thermosets based on PCL and polyethylene glycol (PEG) of different molecular weights were synthesized via photo-cross-linking of methacrylate macromonomers.<sup>54</sup> The different melting temperatures of PEG and PCL were used to develop the PEG-co-PCL thermoset with a two-way shape-memory effect (SME).54 Fan et al. recently developed biodegradable high-performance triboelectric nanogenerators (TENGs) based on blending of PCL and ethyl cellulose (EC) material.<sup>55</sup> The low polymerization rate of PCL was significantly improved by EC, and the poor mechanical properties of EC was improved greatly by PCL. The PCL/EC blend with 6 wt % EC was found to have a maximum power density of 157.17 mW/m<sup>2</sup>. The good elasticity and high tensile strength as well as the remarkable stability and biodegradability of the PCL/EC TENG make it possible for it to be attached on the human body as a comfortable wearable motion sensor and in energy-harvesting applications.

This work reports in situ polymerization and compatibilization of ESO with PCL in a homogeneous solution of chloroform at room temperature using BF<sub>3</sub>·OEt<sub>2</sub> as a cationic initiator. The advantage of this blending technique is attributed to the use of the polymerization/cross-linking reaction that can be performed in a homogeneous solution. It is expected that this method enables better control of phase behavior and thereby the formation of nanoscale morphology, which is not accessible by the conventional blending methods, such as melt blending and solvent casting. A well-defined semi-interpenetration polymer network of PCL/ESO with different crystallization behaviors, nanomorphologies, SMEs, and biocompatibilities was explored with different blend concentrations in this study. The materials were analyzed by differential scanning calorimetry (DSC), DMA, thermogravimetric analysis (TGA), and transmission electron microscopy (TEM). The SMEs of the blend was tested by the thermocycle method. Furthermore, the cell compatibility of the materials was also tested by seeding human umbilical vein endothelial cells (HUVECs) on the blend surface and observing cell attachment by confocal laser scanning fluorescence microscopy (CLSFM).

## **EXPERIMENTAL SECTION**

Materials. ESO was purchased from Elf Atochem Inc., Philadelphia, PA. It was used as received without any treatment. PCL was provided by the Union Carbide Corporation (PCL-767). The weight-average molecular weight of PCL is 40,400 g/mol, and polydispersity is 2.61. Boron trifluoride diethyl etherate, the cationic initiator, BF<sub>3</sub>·OEt<sub>2</sub>, and chloroform were purchased from Sigma-Aldrich Chemical Inc. Medium 200 and Low Serum Growth Supplement, 0.25% trypsin-EDTA (1x), trypsin neutralizer solution, Dulbecco's phosphate buffered saline (PBS), fetal bovine serum, and penicillin-streptomycin (10,000 units/mL of penicillin and 10,000  $\mu$ g/mL of streptomycin) were purchased from Gibco. HUVECs (pooled donor) and the growth factor reduced Matrigel matrix were purchased from Corning. The reagent diluent (10x) was purchased from R&D Systems. The 16% w/v methanol-free paraformaldehyde solution, Hoechst 33342, Alexafluor 488-labeled goat antimouse IgG, and Fluorescein-Phalloidin were purchased from Invitrogen. The mouse antihuman vinculin antibody was purchased from EMD Millipore. Transparent 96-well polystyrene microplates were purchased from Nunc. The four well-glass-bottom dishes were purchased from Matsunami Glass.

Sample Preparation. The semi-interpenetrating PCL/ESO polymer network of different compositions was prepared via in situ polymerization and compatibilization of ESO in a homogeneous solution of PCL and chloroform. Different concentrations of PCL were dissolved in chloroform at room temperature. The cationic initiator (BF<sub>3</sub>·OEt<sub>2</sub>) was mixed with the PCL-chloroform solutions. The concentration of BF3 OEt2 was kept constant at 2 wt % relative to the concentration of ESO. ESO was added to the homogeneous mixture of BF<sub>3</sub>·OEt<sub>2</sub>, chloroform, and PCL dropwise with continuous stirring. Chloroform is an excellent solvent for ESO, BF<sub>3</sub>·OEt<sub>2</sub>, and PCL. Therefore, a homogeneous solution of 25 wt % solid in chloroform can be easily prepared. In addition, the extremely fast ringopening polymerization of ESO using the BF<sub>3</sub>·OEt<sub>2</sub> cationic initiator started immediately after completing the mixing process, forming a yellow gel (semi-interpenetrating network) without any reduction in the volume. The yellow gels of different concentrations were left to dry in air at room temperature for 3 days and under vacuum at 60 °C for another 24 h. The chloroform used in the mixing process was recycled and reused for different purposes. The exothermic cationic ring-opening polymerization of ESO was significantly inhibited in chloroform. This blending technique cannot be performed without chloroform, which is a good solvent for PCL, ESO, and BFE.

**DMA Measurements.** The DMA measurements for the PCL/ESO semi-interpenetrating network of different concentrations were studied using a Q800 dynamic mechanical analyzer from TA Instruments in Tension mode. Rectangular samples with approximately 8 mm width, 1.0 mm thickness, and 13 mm length were heated from –70 to 40 °C at a 2 °C min $^{-1}$  heating rate. All the DMA measurements were carried out at a displacement amplitude of 5  $\mu$ m and a 1 Hz frequency. The glass relaxation processes ( $\alpha$ -relaxation) obtained from the peak maximum of tan d were used to evaluate the phase behavior and miscibility of the blends.

**DSC and TGA Measurements.** The DSC measurements were investigated using a Q2000 differential scanning calorimeter from TA Instruments. All DSC thermograms (heating and cooling) were studied under a dry nitrogen atmosphere. The thermal history of all samples was erased by rapidly heating the samples to 100 °C and keeping the samples at this temperature for 3 min. The samples were then cooled to -80 °C at a 10 °C/min cooling rate followed by heating to 100 °C at a 10 °C/min heating rate. In the second heating run, the melting temperature ( $T_{\rm m}$ ) was determined from the endothermic melting peak maximum. The crystallization temperature ( $T_{\rm c}$ ) was determined from the minimum of the exothermic crystallization peak during the cooling run at a 10 °C cooling rate.

The TGA measurements were investigated by using a Q50 thermogravimetric analyzer (TA Instruments, New Castle, DE). The samples of different concentrations but almost constant weight of 5 mg were heated from 200 to 600 °C at a 20 °C/min heating rate under a nitrogen atmosphere. The thermal degradation temperature for each sample was evaluated from the onset temperature at which the weight loss % starts to decrease.

**TEM and WAXS Measurements.** The nanoscale morphologies of the PCL/ESO semi-interpenetrating network were investigated using a transmission electron microscope (a JEOL JEM-1400 TEM system operating at 120 kV). Ultrathin films of approximately 70 nm thickness using a Reichert–Jung ultracryomicrotome with a diamond knife were prepared for all samples. All the thin films were then stained by RuO<sub>4</sub> vapor for 2 h to improve the contrast of the two-phase nanomorphology.

The wide-angle X-ray scattering (WAXS) was investigated using a Xeuss 2.0 SAXS/WAXS equipped with a microfocus sealed copper tube and a Pilatus3 R200 K detector (83.8 × 70.0 mm with 200,000 pixels). The wavelength of the X-ray was 1.54 Å (0.6 mA and 50 kV), while the sample to detector distance for the WAXS was 0.156 m. The exposure time was 2 min, and scattering reflections were collected under vacuum at room temperature. The beam size was 1.5 mm, and the X-ray scattering points correspond to the center of the beam. The beam size covers  $\pm 3.8 \text{ s}^{-1}$  for each measuring point. In addition, the patterns of the WAXS were analyzed using Igor Pro software with the Nika 2D SAS macros package (Wave Metrics, Portland, OR).

**Infrared Spectroscopy (FT-ATR-IR).** The IR spectra were measured on a Bruker Vertex 80 spectrometer instrument as solids in attenuated total reflectance (ATR) mode using a Harrick diamax with a diamond ATR crystal. A total of 32 scans were collected and the resolution was 1 cm<sup>-1</sup>.

**Confocal Laser Scanning Fluorescence Microscopy.** Fluorescent images were acquired on an Olympus FluoView FV1000-D confocal laser scanning fluorescence microscope equipped with 405, 473, 559, and 635 nm lasers.

**Shape-Memory Effect.** SME was demonstrated for the semi-interpenetrating network of PCL/ESO solid spiral shape. The spiral temporary shape was fabricated at 60 °C from a plane stripe and then fixed by cooling the sample in an ice water bath. The temporary spiral shape recovered into its permanent shape (plane stripe) within just 16 s once the sample was heated by immersion in a water bath at 60 °C. **Cell Culture on the PCL/ESO Substrates.** The PCL, PCL/ESO and ESO network polymers were cut into disk shape using a hollow punch ( $\phi$  5.2 mm) and immersed in 70% ethanol/water overnight. After blotting 70% ethanol/water, the disks were irradiated with a UV lamp for 15 min inside the biosafety cabinet. The disks were placed in a 96-well plate (one disk per well) and dried overnight. Then, the disks were immersed in 2% growth factor reduced Matrigel/PBS, and

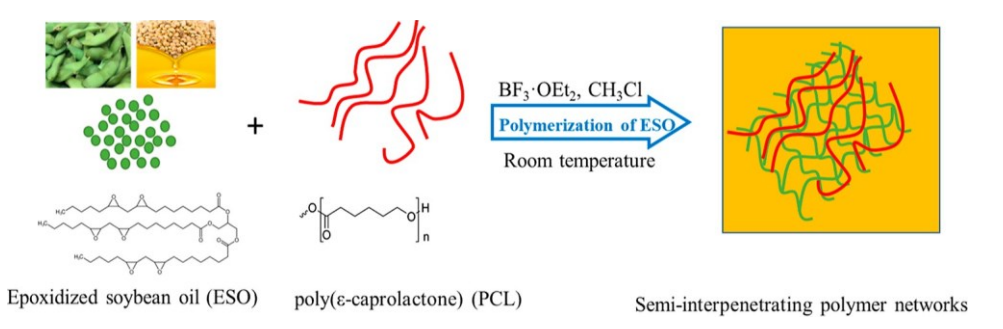


Figure 1. Collective figure for soybean plant and epoxidized soybean oil and poly(*e*-caprolactone) chemical structures as well as schematic diagram for the formation of PCL/ESO semi-interpenetrating network after cationic polymerization of ESO at room temperature in PCL-chloroform homogeneous solution using BF<sub>3</sub>·OEt<sub>2</sub> initiator.

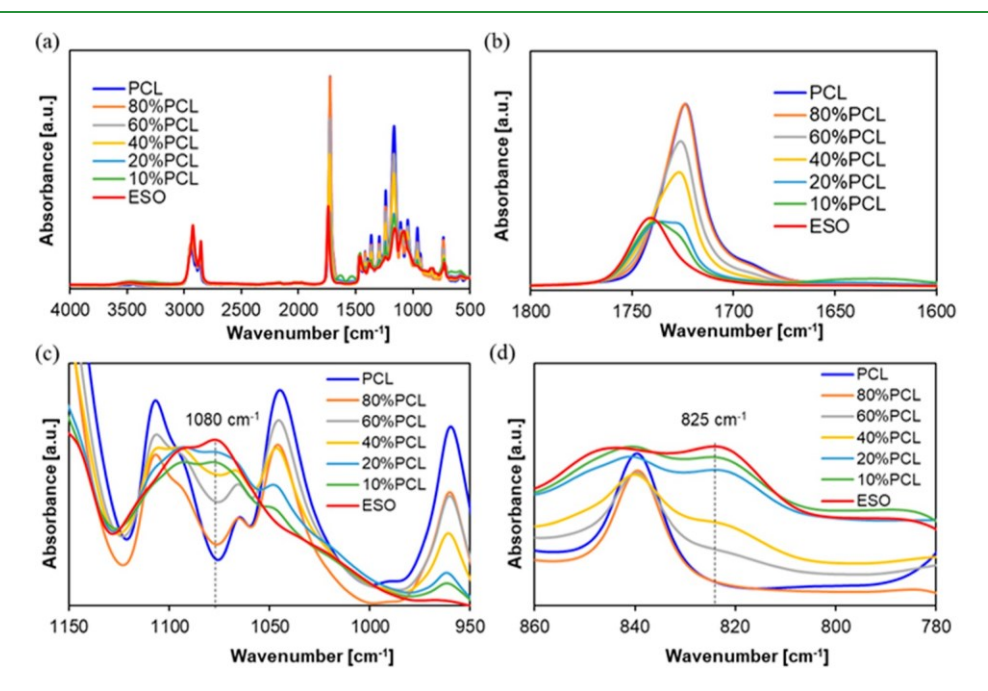


Figure 2. IR spectra of PCL, cured ESO and PCL/ESO network polymers. (a)  $4000-500 \text{ cm}^{-1}$  (b)  $1800-1600 \text{ cm}^{-1}$  (C $\square$ O stretching), (c)  $950-1150 \text{ cm}^{-1}$  (C $\square$ O asymmetric stretching due to epoxide), (d)  $780-860 \text{ cm}^{-1}$  (C $\square$ O symmetric stretching due to epoxide).

incubated at 37 °C for 30 min. After the Matrigel solution was discarded using a micropipette, HUVECs were seeded on the disks at  $1 \times 10^4$  cells/well (medium: 100  $\mu$ L/well) and cultured for 1 day in a CO<sub>2</sub> incubator. As a positive control, cells were also seeded in a Matrigel-coated glass-bottom dish at the same seeding density. After the medium was removed, the disks were immersed in 4% paraformaldehyde (200 µL/well) for 15 min at RT, washed with PBS three times, and immersed in fresh PBS. Cells were permeabilized with 0.2% Triton X-100/PBS for 15 min and blocked with 1% BSA/PBS (Reagent diluent) for 1 h. Actin filaments were stained with fluorescein-phalloidin (1:400 dilution with a reagent diluent) for 1 h. Vinculin was stained with antihuman vinculin antibody (1:50 dilution with reagent diluent) for 1 h and thereafter Alexafluor 488-labeled goat antimouse IgG (1:200 dilution with reagent diluent) for 1 h. Nuclei were stained with Hoechst 33324 (1:2000 dilution with PBS) for 15 min. For each step, the samples were washed with PBS three times. The fluorescence images were collected by CLSFM.

# RESULTS AND DISCUSSION

Polymer blends can be classified as miscible with one phase structure, immiscible or incompatible with two phase morphologies and irregular coarse structure, as well as unstable domain sizes with sharp and weak interfaces.<sup>56–59</sup> Compatible

blends have a finer morphology with better interfacial adhesion and good mechanical properties compared to the immiscible ones. Prediction and control of the structure evolution in the blends are still elusive goals in polymer science. The inability to reduce the particle size and improve the interfacial interaction between the two phases precluded polymer blends from many industrial applications due to their poor overall mechanical and physical properties. This problem can be solved by using block, graft, or star copolymers as compatibilizers. These types of compatibilizers are known to migrate to the interface, reduce surface tension, and consequently increase the thermodynamic stability of the morphology of the immiscible blends. Regardless of the important role of compatibilizers to control the phase behavior, morphology, and properties of polymer blends, they are very expensive, cannot be prepared in large quantities, and are generally not available commercially. Therefore, there is a need to develop more effective and alternative methods to produce a fine morphology and excellent properties in polymer blends. In situ polymerization and compatibilization of polymer blends during mechanical mixing and molding are strategies that allow for control of the phase domain interface, consequently yielding small domain sizes with enhanced

Table 1. Absorption Maxima in the  $\mathbf{v}(C \square O)$  Stretching Vibration Region as Well as the  $T_{gs}$ ,  $T_{m}$ ,  $T_{c}$ , DOC,  $T_{onset}$ , and wt % of Residual Materials at 480 °C for PCL/ESO Blends of Different Concentrations

PCL wt %	$V(C\square O)/cm^{-1}$		Tg (PCL)/°C	$T_{\rm g}$ (ESO)/°C	$T_{\rm m}/{}^{\circ}{\rm C}$	$T_c/^{\circ}C$	DOC	$T_{\mathrm{onset}}/^{\circ}\mathrm{C}$	wt % at 480°C
100	1724		<b>-</b> 55		60	25	50.1	380	4
80	1724		-52	-12	58	3	48.5	380	8
60	1726				55	3	37.5	375	8
40	1728		-45	-7	53	<b>-</b> 15	30.0	375	15
20	1728 (shoulder)	1735	-28	-10	51	-20	12	375	15
10	1728 (shoulder)	1737		<b>-</b> 5	49.5	<b>-2</b> 1	5.0	375	17
0	1724	1741					0.0	375	21

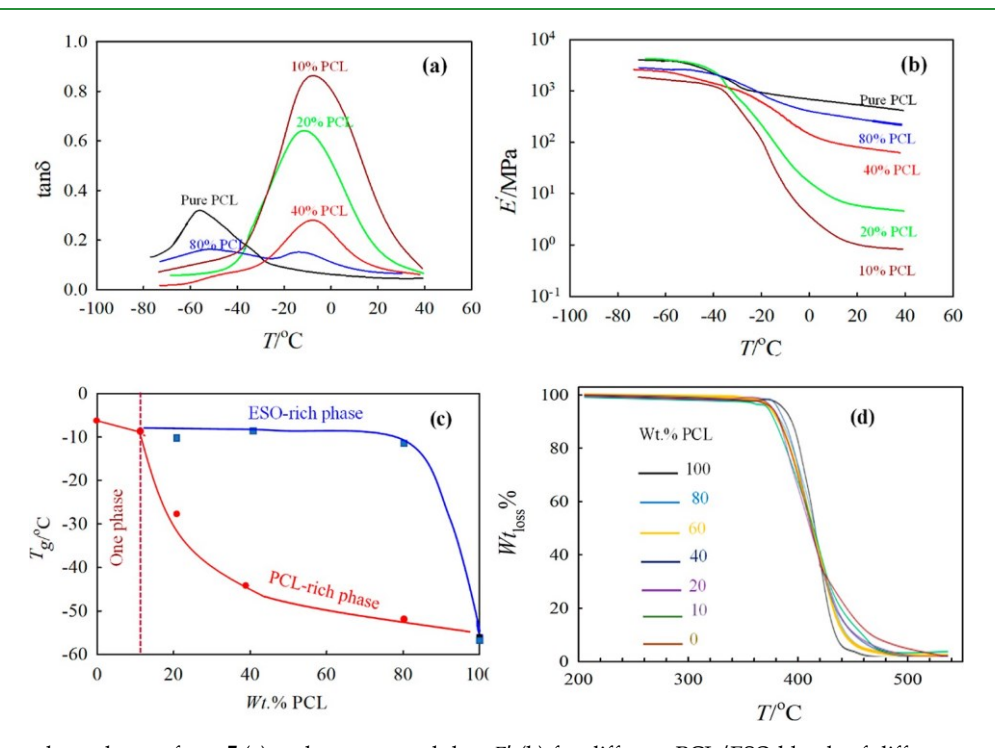


Figure 3. Temperature dependence of  $tan \delta$  (a) and storage modulus, E' (b) for different PCL/ESO blends of different compositions at 1 Hz frequency and 2 °C/min heating rate. (c) Composition dependence of  $T_g$  obtained from the peak maximum of  $tan \delta$  of Figure 3a. (d) TGA measurements for different PCL/ESO blends of different compositions at 20 °C/min heating rate.

benefits. In this article, we illustrate this general strategy and demonstrate its feasibility for PCL and ESO blend to create stable nanoscale morphologies.

Figure 1 shows the soybean plant and the chemical structure of the epoxidized soybean oil. The semi-interpenetrating PCL/ ESO network was also described schematically in Figure 1, where the green ESO was mixed with PCL in chloroform and BF<sub>3</sub>·OEt<sub>2</sub> initiator. The ring opening polymerization of ESO started rabidly in the homogeneous solution to create semiinterpenetrating network with a unique phase behavior and nanoscale morphology that would not be achieved with conventional blending methods, such as melt blending and solution casting. The red solid lines are the PCL chains and green network are the three-dimensional cross-linked structure of ESO. To cross-link ESO, we used photoinitiated cationic polymerization of ESO, which was originally reported by Crivello and Narayan. 60 The nature of the cation and the anion of the photo initiator were found to have a significant effect on the polymerization rates. The epoxy content in the epoxidized soybean oil also strongly influences the photoinitiated cationic polymerization rate. The obtained ESO-based network was characterized by a thermal and mechanical techniques.

Figure 2a shows the FTIR spectra for the PCL/ESO semiinterpenetrating network of different concentrations. As shown in Figure 2b and Table 1, in the spectral range of 1800–1600 cm<sup>-1</sup>, we observed the carbonyl stretching vibrations of the ester groups present in both ESO and PCL. The peak maximum is 1724 cm<sup>-1</sup> for PCL and 1741 cm<sup>-1</sup> for ESO, respectively. For the PCL/ESO blends, with the increase in the weight ratio of ESO, the increase in the absorbance at around 1741 cm<sup>-1</sup> was observed. Furthermore, as shown in Figure 2c,d, we observed the peaks at 825 and 1080 cm<sup>-1</sup> corresponding to C-O-C symmetric and asymmetric stretching of epoxide groups, respectively.61 Those peaks were observed for both the cured ESO and PCL-ESO blends containing 10-60 wt % PCL, indicating the presence of unreacted epoxide groups in those samples. The spectrum of the cured ESO was further compared with that of the reported uncured ESO.62 As shown in Figure 1, compared to the uncured ESO, the relative absorbance of the peaks at 825 cm<sup>-1</sup> (epoxide) compared to 725 cm<sup>-1</sup> (C-H bending) was smaller for the cured ESO showing that the ring opening of the epoxide group occurred during the curing process.

Figure 3a,b demonstrate the DMA storage modulus E' and the loss tangent tan  $\delta$  at different temperatures for PCL/ESO

semi-interpenetrating network of different compositions. For cured blends of low PCL contents of up to 10 wt % PCL, only one  $\alpha$ -relaxation peak (tan  $\delta$  maximum) was observed indicating that the semi-interpenetrating network with PCL contents lower than or equal to 10 wt % can form a single miscible blend. The  $\alpha$ -relaxation process is mainly related to the cooperative motion of the polymeric chains under the applied oscillatory deformation during the DMA measurement and is associated with the  $T_g$  of the material. With higher PCL content, two α-relaxation peaks, one for ESO-rich phase (higher  $T_g$  phase) and one for PCL-rich phase (lower  $T_g$ phase) were observed. In addition, the intensity of the tan  $\delta$ peak maximum decreases significantly with increasing PCL content. It is also clear that the difference between the peak maxima of the two rich phases increases in magnitude with increasing the PCL content. For example, the peaks of the  $\alpha$ relaxation process of ESO-rich and PCL-rich phases are -12 and -52 °C for blend of 80 wt % PCL, respectively. Although, the peak maximum of the  $\alpha$ -relaxation process of PCL-rich phase changed with blend composition, the peak maximum of the ESO-rich phase changed only slightly, as shown in Table 1. This experimental fact suggested that the PCL-rich phase has a certain amount of ESO partially miscible due to the increase in the temperature of the peak maximum of tan  $\delta$ . The amount of ESO in the PCL-rich phase (i.e., amount of ESO dissolved in PCL rich-phase) increases with increasing content of ESO in the blend. The tan  $\delta$  peak maximum of ESO-rich phase was slightly changed indicating that the amount of PCL dissolved in the ESO-rich phase is very small. It must be stated that the low intensity and broadness of the peak maximum of tan  $\delta$  for the PCL-rich phase led to inaccurate determination of the  $T_{\rm g}$ and consequently the evaluation of blend miscibility of the two components based on the DMA measurements is inaccurate as well. Therefore, the miscibility of these blends was further investigated from the morphology of the blends by highresolution TEM as described later in this section.

At low temperature (-70 °C) in the glassy state, the value of E' of the PCL/ESO blends was found to be composition dependent. The value of E' increased with increasing the content of PCL and reached a maximum value at 20 wt % PCL as clearly seen in Figure 3b. The ESO thermoset is a very elastic material with a low  $T_g$  of about -4 °C. While the PCL is a rigid semi crystalline material with a melting point of 60 °C. This is why the elastic modulus at low temperature decreased by adding ESO. However, the  $T_g$  of PCL is about -60 °C, as shown in DMA itself and it is not a rigid polymer. 63,64 At a higher temperature, the blends reached a plateau. The E' value at a plateau decreases with decreasing the PCL content in the blend. This plateau is related to the combination of both crystallinity and cross-link density of the blend. The effect of ESO on the crystallization behavior was investigated using DSC and WAXS as discussed later in this paper. It appears that the in situ polymerization and compatibilization of ESO and PCL in homogeneous solution produced unique semi-interpenetrating network with thermomechanical properties that are strongly influenced by the concentration of PCL in the blends. The optimum value of E' in the glassy state for blend with 20 wt % PCL might be related to a unique nanoscale morphology and must be investigated by TEM as will be discussed later in this paper.

The  $T_g$  obtained from the peak maximum of the  $\alpha$ relaxation process (DMA data in Figure 3a) is presented as a function of blend composition in Figure 3c. Clearly, one  $T_g$  for

blend concentrations of PCL ≤10 wt %. While, on the other hand, two- $T_{\rm gs}$  (two-phase regimes) can be seen at PCL concentrations  $\geq 10$  wt %. The difference between the two  $T_{\rm gs}$  $(\Delta T_g = T_{gESO} - T_{gPCL})$  of the two rich phases was also found to be composition dependent. The higher the concentration of PCL the larger the difference between the two  $T_{\rm gs}$  as clearly seen in Figure 3c and Table 1. Based on this finding, it appears that the partial miscibility of PCL and ESO thermoset decreases significantly with increasing the concentration of PCL. The internal structure or morphology of this system must be investigated using TEM to get a deeper insight into understanding the phase behavior and miscibility of the two polymer components. For the effect of the ESO thermoset on the thermal stability of the PCL/ESO blends, the TGA measurements were carried out from 200 to 600 °C at a 20 °C/min heating rate under a nitrogen atmosphere. The thermal degradation temperature for each sample was determined from the onset temperature ( $T_{\text{onset}}$ ) at which the weight loss % starts to decrease. As shown in Figure 3d and Table 1, the *T*<sub>onset</sub> decreased from 380 °C for both the pure PCL and PCL/ESO 80/20 blend to 375 °C for all other blends. It is also clear that the concentration of the residual material at 480 °C increased significantly from 4 wt % for pure PCL to up to 21 wt % for pure ESO.

We next observed the fine morphology of the blends by high-resolution TEM in order to understand the effect of in situ polymerization and compatibilization of ESO with PCL on the phase behavior and miscibility. Figure 4 shows the TEM

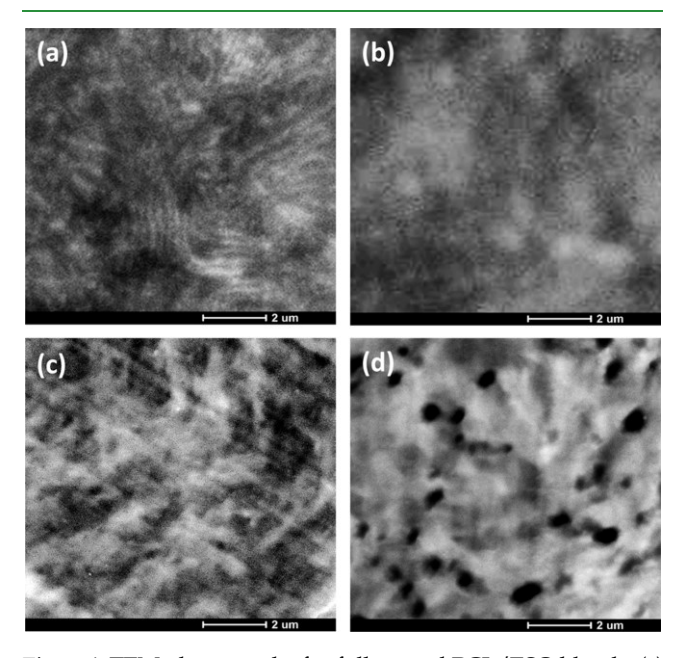


Figure 4. TEM photographs for fully cured PCL/ESO blends: (a) PCL/ESO 10/90, (b) PCL/ESO 20/80, (c) PCL/ESO 40/60, and (d) PCL/ESO 80/20.

photographs for the different blend compositions of the PCL/ESO blends. The blends with 10 and 20 wt % PCL showed lamellar and or micelles-like structure commonly seen in multiblock copolymers. The dark phase is the ESO thermoset while the bright one is the PCL phase. The TEM photographs are not clear enough to confirm miscibility or phase separation between the two polymer components in the low PCL concentration range. For the blends with higher PCL concentrations, a clear two-phase morphology was observed.

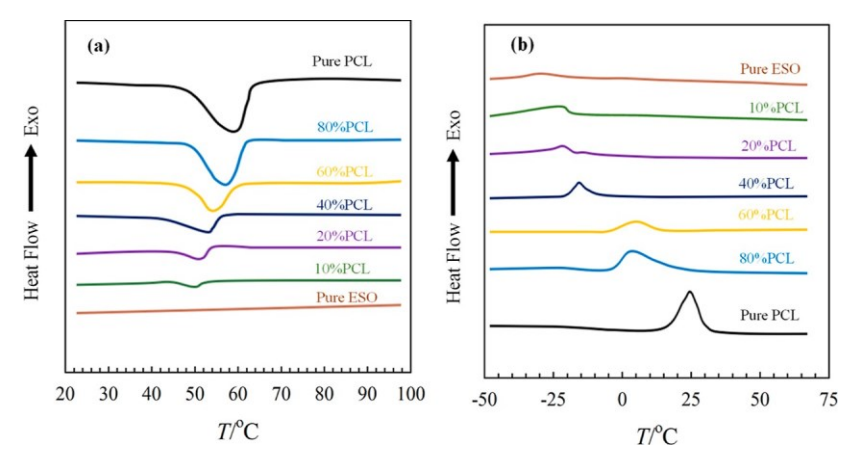


Figure 5. DSC thermograms for PCL/ESO blends of different concentrations: (a) second heating run, where the endothermic peaks are the melting peaks of PCL in different blends, (b) cooling run, where the exothermic peaks are related to the crystallization of PCL in different blends. The measurements were carried out at 10 °C/min heating and cooling rates.

For example, a cocontinuous microstructure of the two phases was observed for PCL/ESO = 40/60 blend (Figure 4c). On the other hand, for the blend at PCL/ESO = 80/20, a dark ESO particle with nanoscale morphology of approximately 500 nm dispersed in a bright PCL matrix (Figure 4d). The results show that the in situ polymerization and compatibilization of PCL/ESO blends produced different miscibility and phase behavior, including miscible and interconnected cocontinuous structure, as well as partially miscible with nanoscale morphology, and the unique combination of thermal and thermomechanical properties that are not possible to obtain using conventional blending techniques, such as melt mixing and solution casting method. These unique structures and properties of the nanoblends of PCL/ESO might be beneficial for preparing multifunctional polymeric systems.

The phase separation in semi-interpenetrating polymer network has been widely observed in many systems in literature. 65-69 For example, spinodal decomposition phase separation in polystyrene and cross-linked polymethacrylate semi-interpenetrating polymer network was reported by Møller et al.65 Liquid-liquid phase separation via spinodal decomposition of an atactic polystyrene solution in methacrylate monomers was obtained during the gelation process of the polymer-rich phase. The phase separated structure was permanently stabilized by low-temperature cross-linking of methacrylate monomers via UV polymerization and the morphology was investigated using TEM. Similarly, semiinterpenetrating poly(L-lactide) and diisocyanate-bridged 4arm star-shaped ε-caprolactone oligomers has been successfully synthesized by Shibata et al.66 They found that the semiinterpenetrating polymer network has microphase separation, but the 50/50 blend composition showed the finest phase separated morphology. Based on the above it is not surprised at all to see nanoscale morphologies in the PCL/ESO semiinterpenetrating network (see Figure 4).

Blending semi crystalline and amorphous polymers often produces significant changes in the structural parameters of the crystals, such as spherulitic growth rates, crystal interphase, and lamellar thickness. It is also common to see a depression in the crystallization kinetics, heat of fusion, and melting point of the semicrystalline component in miscible polymer blends. On the other hand, enhancement in the crystallization process can be observed for heterogeneous polymer blends with fine morphology. The elevation or depression in the crystallization

process are governed by the interaction between the amorphous and semicrystalline polymer components and by the change in the free energy required to form crystals. The thermal history of all samples was erased by annealing the samples in a melt at 100 °C for 3 min. For the first heating run, the samples were cooled to -80 °C at a 10 °C/min cooling rate followed by heating to 100 °C at a 10 °C/min heating rate. The melting temperature ( $T_{\rm m}$ ) of all samples was determined from the endothermic melting peak maximum during the second heating run (from -80 to 100 °C at 10 °C/min cooling rate). The crystallization temperature ( $T_{\rm c}$ ) was determined from the minimum of the exothermic crystallization peak during cooling the samples at a 10 °C cooling rate. The values of both  $T_{\rm m}$  and  $T_{\rm c}$  for all blends of different concentrations are summarized in Table 1.

Figure 5a shows the thermograms of the second heating run for the PCL/ESO blends of different concentrations. The thermogram of pure ESO thermoset has no melting peak because ESO is a totally amorphous component. The melting peak is related to the PCL component. Clear melting peaks were observed for all other PCL/ESO blends. The melting peak systematically shifted to a lower temperature with the increase of the ESO concentration in the blends. This systematic variation in the melting point of PCL with the increase of the ESO concentration indicates that PCL and ESO are miscible or partially miscible and have favorable intermolecular interaction. It is also clear that the heat of fusion (area under the melting peak) is significantly decreased with the increase in the ESO concentration in the blend. Similar behavior has been observed in the crystallization behavior of the blends during the cooling run at 10 °C/min cooling rate as seen in Figure 5b. The crystallization temperature shifted to lower temperatures, and the crystallization enthalpy (area under the DSC crystallization peak) significantly decreases with the increase of the ESO concentration in the blends.

To get more detailed information about the crystallization behavior of PCL in the PCL/ESO blends, the samples were measured by WAXS. As mentioned above, the crystallization behavior of semi crystalline polymer can be significantly influenced by the amorphous polymer in blend. The effect is expected to be more significant when the semi crystalline polymer is blended with an amorphous thermoset polymer as in the current system. The degree of crystallinity can be

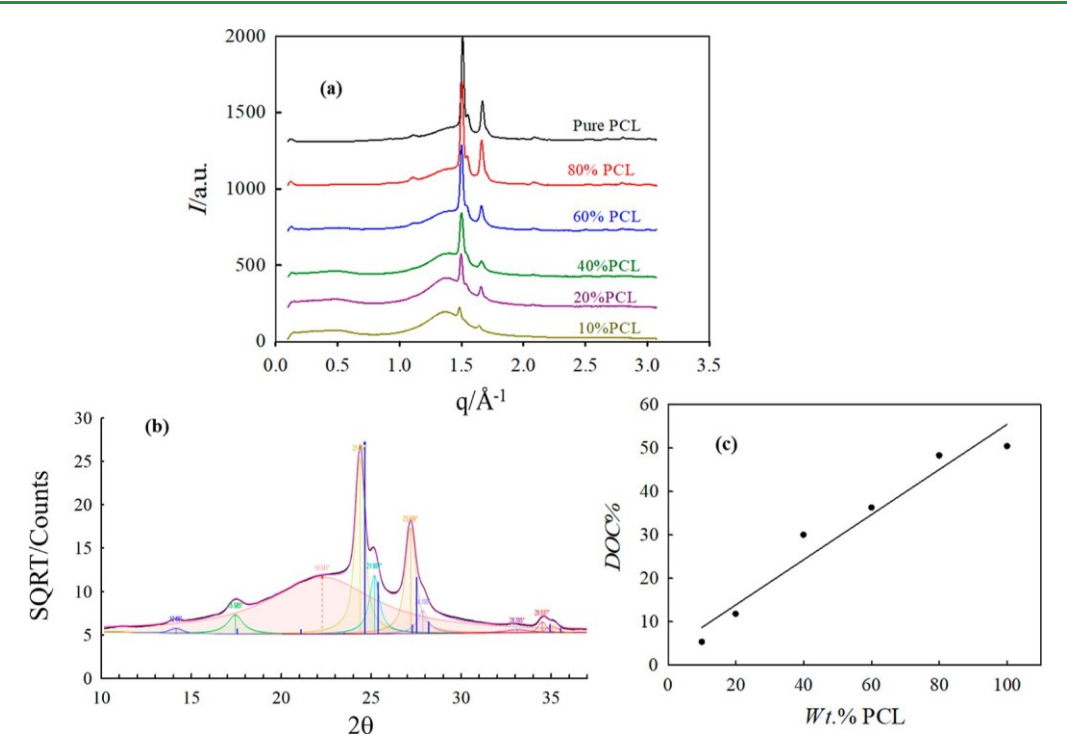


Figure 6. (a) WAXS patterns for PCL/ESO blends of different concentration. (b) Analysis of the WXS pattern for PCL/ESO 80/20 wt % blend. (c) Composition dependence of degree of crystallinity (DOC) for PCL/ESO blends calculated from the analysis of WXS patterns.

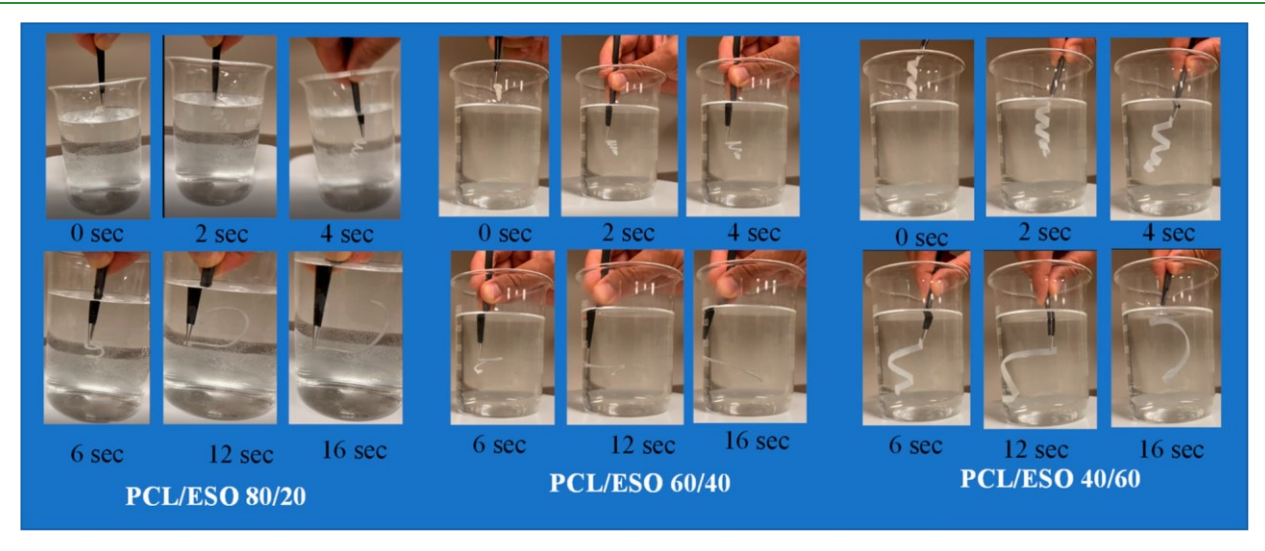


Figure 7. SME for different blend compositions induced by thermal heating. The spiral temporary shape recovered completely (16 s) into its plane stripe permanent shape once the sample was immersed in a beaker with hot water at 60 °C.

evaluated accurately from the WAXS pattern. By WAXS, any crystallinity in the system, even with small crystallinity content, can be detected. Figure 6 shows the WAXS patterns for the PCL/ESO blends at different concentrations. A sharp scattering peaks with high intensities were detected at  $2\theta$  = 21.38 and 23.68 for the different samples. These two main reflection peaks are not significantly changed with the blend composition and are typically related to the orthorhombic crystalline structure of cell with (110) and (200) reflections. The degrees of crystallinity can be accurately calculated from the analysis and integration of WAXS spectrum as seen in Figure 6b (PCL/ESO 80/20 wt % blend). The obtained degree of crystallinity increases linearly with increasing content of PCL in the blend (Figure 6c and Table 1).

**Shape-Memory Effect.** SME is a unique dynamic phenomenon developed especially for smart medical devices, such as cardiac pacemakers, stents, or surgical sutures. According to the SME, the shape memory polymer (SMP) can be fixed temporarily in a certain mechanically deformed shape under a certain condition at a constant deformation temperature. The SMP will return to its original shape only when exposed to a suitable stimulus such as heat or light. The SMP can simply be exposed to heat or light directly. Indirect heat can be achieved via an alternating magnetic field. The medical devices made from SMP can be deformed and implanted in its temporary small shape and will recover its original large shape in the patient's body. One advantage of biodegradable SMP is that the material will be degraded in the

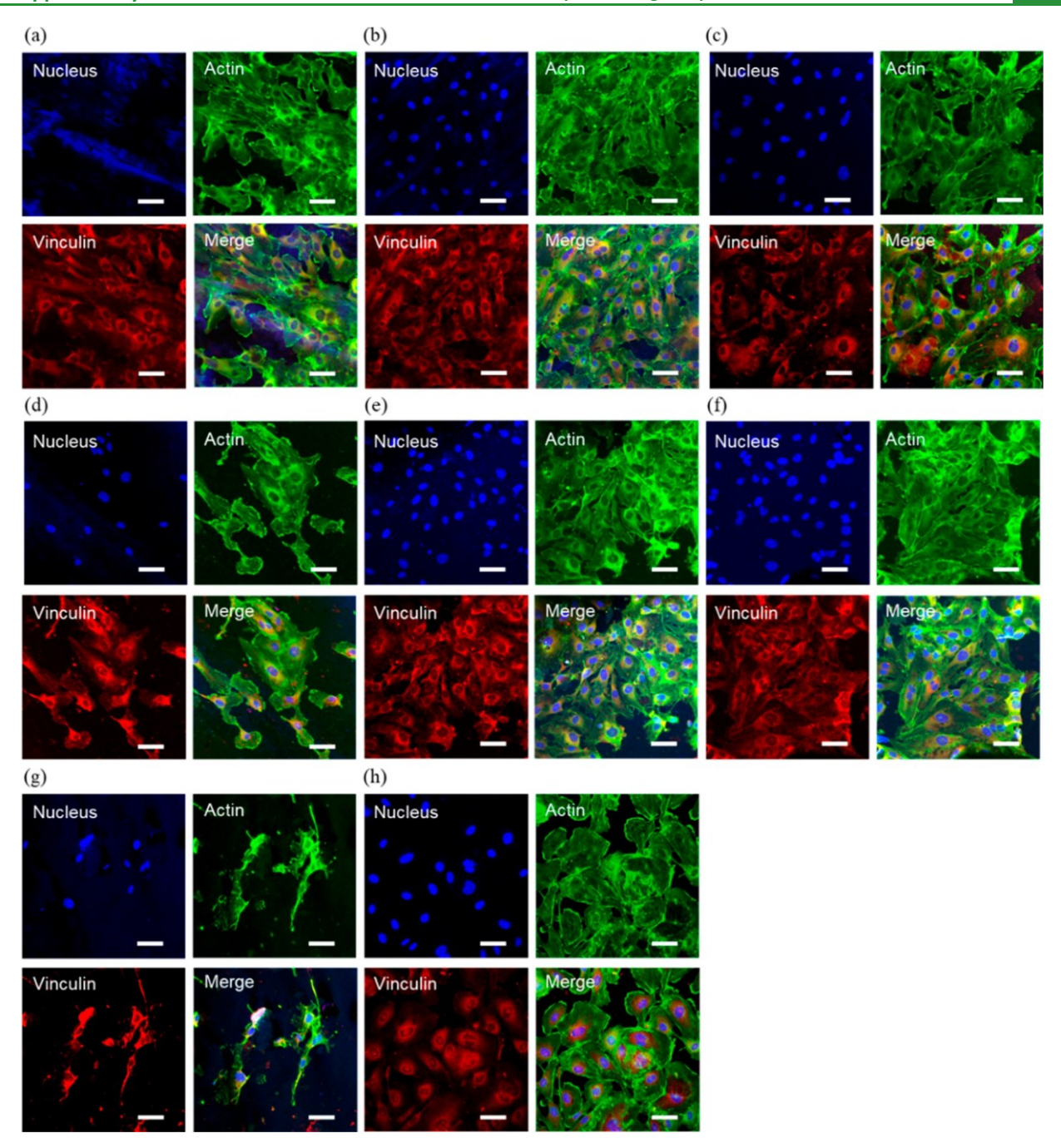


Figure 8. Cell attachment on different substrates. HUVECs were seeded onto (a) PCL, (b-f) PCL/ESO, (g) ESO, and (h) glass and cultured for 1 day. Cells were fixed, stained, and observed by CLSFM. PCL/ESO ratios: (b) 80/20, (c) 60/40, (d) 40/60, (e) 20/80, and (f) 10/90. Scale bars:  $50 \mu m$ .

ı

body, and consequently, there is no need for a second surgery for device explanation. For the PCL/ESO semi-interpenetrating network, the SME can be achieved based on the switching domains of the PCL crystals, and the fixed domains are related to the cross-link structure of ESO. The programming of the SME is a process based on the combination of polymer morphology and architecture with a well-defined thermomechanical procedure. Physical or chemical cross-links can be used to define the permanent shape of the SMP. The temporary shape is normally fixed by solidification of the switching domains by either crystallization or vitrification. Thermally induced SME is the most common one, and the polymer recovers to its original shape when the heat exceeds

the switching temperature associated with the thermal transition of the switching domains (melting temperature of PCL in the current system). The SME of different PCL/ESO blend compositions for a temporary fixed spiral shape is shown in Figure 7. The permanent plane stripe shapes were deformed into a spiral shape at a programming temperature at 60 °C and slightly above the melting temperature of the PCL-rich phase in the blend. The temporary shape was fixed by quenching (i.e., cooling very rapidly) the blends from 60 to 0 °C in an ice water bath (beaker). The fixed temporary spiral shapes returned to their plane stripe permanent shape very quickly (in 16 s) once the samples were immersed in a beaker with hot water at 60 °C as can be seen in Figure 7. This test was

repeated three times for each composition, and we obtained identical data. Temperature of the water was checked with a thermometer before immersing the samples in water.

Biocompatibility of the PCL/ESO Blends. SMPs can be used to develop medical devices such as coronary stents,<sup>70</sup> endovascular embolization devices,<sup>71</sup> sutures,<sup>72</sup> and drug delivery systems.<sup>73</sup> For biomedical applications, it is of importance to test the safety as well as cell compatibility of the materials. Here, we evaluated the adhesion of HUVECs on the PCL/ESO blends, which is one of the key biocompatibility requirements for devices in direct contact with blood.74 In this experiment, HUVECs were seeded onto the PCL/ESO blends and cultured for 1 day. Then, vinculin and actin filaments were stained immunohistochemically. Vinculin is a component of focal adhesions and adherent junctions, and actin filaments are a component of the cytoskeleton. Formation of focal adhesions and organization of actin filaments are essential for cell adhesion, migration, and division. As shown in Figure 8, we observed that HUVECs attached and stretched on the PCL surface whereas only a few cells were found on the ESO surface. The cell density on the PCL surface was similar to that of a glass surface (positive control), showing that the PCL polymer prepared in this study is not toxic. The PCL/ESO surfaces at different compositions show cell attachment similar to that of the PCL surface. Interestingly, even at high ESO content (PCL/ESO 10/90), HUVECs could attach and spread on the surface. This result indicates that PCL and ESO were mixed at a molecular level, which enhanced surface endothelialization. Formation of a monolayer of endothelial cells on biomaterials is one of the approaches to inhibit blood clot formation. Therefore, PCL/ESO network polymers are promising biomaterials that can be used for cardiovascular devices.

### **CONCLUSIONS**

A semi-interpenetrating PCL/ESO polymer network was successfully prepared via in situ polymerization and compatibilization of ESO in a homogeneous solution of PCL and chloroform. The cationic ring-opening polymerization of ESO started rabidly in the homogeneous solution to create a semiinterpenetrating network with unique phase behavior and nanoscale morphology that would not be achieved with conventional blending methods, such as melt blending and solution casting. For cured blends with lower PCL contents of up to 10 wt %, only one  $\alpha$ -relaxation peak was observed (DMA measurements), indicating that the semi-interpenetrating network with PCL contents ≤10 wt % can form a single miscible blend. With a higher PCL content, two  $\alpha$ -relaxation peaks, one for the ESO-rich phase (higher  $T_g$  phase) and one for the PCL-rich phase (lower  $T_g$  phase), were observed. It was also concluded that the partial miscibility of PCL and ESO thermoset decreases significantly with increasing concentration of PCL. At a low temperature (-70 °C) in the glassy state, the value of E' of the PCL/ESO network was found to be composition-dependent. The value of E' increased with increasing content of PCL and reached a maximum value at 20 wt % PCL. A miscible and interconnected cocontinuous structure as well as being partially miscible with a nanoscale morphology were observed for different blend compositions using TEM. The melting and crystallization temperatures of PCL in the PCL/ESO blends were systematically shifted to lower temperatures with the increase of the ESO component in the blends. This systematic variation in the melting and

crystallization temperatures of PCL with increasing concentration of ESO indicates that PCL and ESO are miscible or partially miscible and have favorable intermolecular interactions in a good agreement with the DMA and TEM results. The degree of crystallinity was accurately calculated as a function of composition from the analysis and integration of the WAXS spectra. The obtained degree of crystallinity was found to be composition-dependent and increased linearly with the increase in the content of PCL in the blends. The PCL/ESO semi-interpenetrating network of different concentrations has excellent thermally induced SME due to the switching domains of the PCL crystals and the fixed cross-link domains of ESO segments. A PCL/ESO 60/40 blend with a fixed temporary spiral shape returned to its plane stripe permanent shape very quickly, in just 16 s, once the sample heated up to its programming temperature. The PCL/ESO semi-interpenetrating network of different concentrations supported endothelial cell adhesion without showing obvious toxicity. Finally, it appears that the in situ polymerization and compatibilization of ESO and PCL in homogeneous solutions produced a unique semi-interpenetrating network with novel thermomechanical, morphological, SME, and biocompatibility that cannot be achieved with conventional blending methods, such as melt blending and solvent casting.

### **AUTHOR INFORMATION**

#### **Corresponding Author**

Samy A. Madbouly – *Pacific Northwest National Laboratory, Richland, Washington 99354, United States;* orcid.org/0000-0002-4903-4362; Phone: 814-898-7169; Email: samy.madbouly@pnnl.gov

#### **Authors**

Setsuko Yamane – Department of Materials Science and Engineering, Pennsylvania State University, University Park, Pennsylvania 16802, United States; National Institute of Technology, Numazu College, Numazu, Shizuoka 410-8501, Japan

André J. van der Vlies – Department of Materials Science and Engineering, Pennsylvania State University, University Park, Pennsylvania 16802, United States

Urara Hasegawa – Department of Materials Science and Engineering and Materials Research Institute, Pennsylvania State University, University Park, Pennsylvania 16802, United States; orcid.org/0000-0002-4189-7630

Complete contact information is available at: https://pubs.acs.org/10.1021/acsapm.3c01270

#### Notes

The authors declare no competing financial interest.



#### **ACKNOWLEDGMENTS**

This work was partially supported by the Pennsylvania State University Research Development Grant (RDG), Engineering Technology and Commonwealth Engineering Research & Engineering Activities with Commonwealth Hubs (REACH) Program. U.H. acknowledges financial support from the U.S. National Science Foundation, CBET, 2102848. S.Y. acknowledges financial support from the National Institute of Technology Faculty Research Abroad Program, Japan.

#### **REFERENCES**

- (1) Umesh, M.; Shanmugam, S.; Kikas, T.; Lan Chi, N. T.; Pugazhendhi, A. Progress in bio-based biodegradable polymer as the effective replacement for the engineering applicators. *J. Cleaner Prod.* 2022, *362*, 132267.
- (2) Taib, N. A.; Rahman, M. R.; Huda, D.; Kuok, K. K.; Hamdan, S.; Bakri, M. K. B.; Julaihi, M. R. M. B.; Khan, A. A review on poly lactic acid (PLA) as a biodegradable polymer. *Polym. Bull.* 2023, *80*, 1179–1213.
- (3) Nita, L. E.; Ghilan, A.; Rusu, A. G.; Neamtu, I.; Chiriac, A. P. New trends in bio-based aerogels. *Pharmaceutics* 2020, *12*, 449.
- (4) Rafiqah, S. A.; Khalina, A.; Harmaen, A. S.; Tawakkal, I. A.; Zaman, K.; Asim, M.; Nurrazi, M. N.; Lee, C. H. A Review on Properties and Application of Bio-Based Poly(Butylene Succinate). *Polymers* 2021, *13*, 1436.
- (5) La Fuente, C. I. A.; Maniglia, B. C.; Tadini, C. C. Biodegradable polymers: A review about biodegradation and its implications and applications. *Packag. Technol. Sci.* 2023, *36*, 81–95.
- (6) Asgher, M.; Qamar, S. A.; Bilal, M.; Iqbal, H. M. Bio-based active food packaging materials: Sustainable alternative to conventional petrochemical-based packaging materials. *Food Res. Int.* 2020, *137*, 109625
- (7) De Gisi, S.; Gadaleta, G.; Gorrasi, G.; La Mantia, F. P.; Notarnicola, M.; Sorrentino, A. The role of (bio) degradability on the management of petrochemical and bio-based plastic waste. *J. Environ. Manage*. 2022, *310*, 114769.
- (8) Åbdeshahian, P.; Ascencio, J. J.; Philippini, R. R.; Antunes, F. A. F.; de Carvalho, A. S.; Abdeshahian, M.; dos Santos, J. C.; da Silva, S. S. Valorization of lignocellulosic biomass and agri-food processing wastes for production of glucan polymer. *Waste Biomass Valorization* 2021, *12*, 2915–2931.
- (9) Sen, K. Y.; Baidurah, S. Renewable biomass feedstocks for production of sustainable biodegradable polymer. *Curr. Opin. Green Sustainable Chem.* 2021, 27, 100412.
- (10) Reshmy, R.; Thomas, D.; Philip, E.; Paul, S. A.; Madhavan, A.; Sindhu, R.; Sirohi, R.; Varjani, S.; Pugazhendhi, A.; Pandey, A.; Binod, P. Bioplastic production from renewable lignocellulosic feedstocks: a review. *Rev. Environ. Sci. Bio/Technol.* 2021, 20, 167–187.
- (11) Vigneswari, S.; Noor, M. S. M.; Amelia, T. S. M.; Balakrishnan, K.; Adnan, A.; Bhubalan, K.; Amirul, A. A. A.; Ramakrishna, S. Recent advances in the biosynthesis of polyhydroxyalkanoates from lignocellulosic feedstocks. *Life* 2021, *11*, 807.
- (12) Adeleye, A. T.; Odoh, C. K.; Enudi, O. C.; Banjoko, O. O.; Osiboye, O. O.; Toluwalope Odediran, E.; Louis, H. Sustainable synthesis and applications of polyhydroxyalkanoates (PHAs) from biomass. *Process Biochem.* 2020, *96*, 174–193.
- (13) Machineni, L.; Rao Anupoju, G. Review on valorization of lignocellulosic biomass for green plastics production: Sustainable and cleaner approaches. *Sustain. Energy Technol. Assessments* 2022, *53*, 102698.
- (14) Ferrari, F.; Striani, R.; Fico, D.; Alam, M. M.; Greco, A.; Esposito Corcione, C. An Overview on Wood Waste Valorization as Biopolymers and Biocomposites: Definition, Classification, Production, Properties and Applications. *Polymers* 2022, *14*, 5519.
- (15) Abe, M. M.; Martins, J. R.; Sanvezzo, P. B.; Macedo, J. V.; Branciforti, M. C.; Halley, P.; Botaro, V. R.; Brienzo, M. Advantages and disadvantages of bioplastics production from starch and lignocellulosic components. *Polymers* 2021, *13*, 2484.
- (16) Jia, P.; Ma, Y.; Kong, Q.; Xu, L.; Li, Q.; Zhou, Y. Progress in development of epoxy resin systems based on biomass resources. *Green Mater.* 2020, 8, 6–23.
- (17) Tremblay-Parrado, K. K.; García-Astrain, C.; Avérous, L. Click chemistry for the synthesis of biobased polymers and networks derived from vegetable oils. *Green Chem.* 2021, *23*, 4296–4327.
- (18) Kurre, S. K.; Yadav, J. A review on bio-based feedstock, synthesis, and chemical modification to enhance tribological properties of biolubricants. *Ind. Crops Prod.* 2023, *193*, 116122.
- (19) Mustapha, R.; Rahmat, A. R.; Abdul Majid, R.; Mustapha, S. N. H. Vegetable oil-based epoxy resins and their composites with bio-

- based hardener: a short review. *Polym.-Plast. Technol. Mater.* 2019, 58, 1311–1326.
- (20) Gonçalves, F. A. M. M.; Santos, M.; Cernadas, T.; Ferreira, P.; Alves, P. Advances in the development of biobased epoxy resins: insight into more sustainable materials and future applications. *Int. Mater. Rev.* 2022, *67*, 119–149.
- (21) Moser, B. R.; Cermak, S. C.; Doll, K. M.; Kenar, J. A.; Sharma, B. K. A review of fatty epoxide ring opening reactions: Chemistry, recent advances, and applications. *J. Am. Oil Chem. Soc.* 2022, *99*, 801–842.
- (22) Joshi, J. R.; Bhanderi, K. K.; Patel, J. V. A review on biolubricants from non-edible oils-recent advances, chemical modifications and applications. *J. Indian Chem. Soc.* 2023, *100*, 100849.
- (23) Pezzana, L.; Melilli, G.; Sangermano, M.; Sbirrazzuoli, N.; Guigo, N. Sustainable approach for coating production: Room temperature curing of diglycidyl furfuryl amine and itaconic acid with UV-induced thiol-ene surface post-functionalization. *React. Funct. Polym.* 2023, 182, 105486.
- (24) Chauke, N. P.; Mukaya, H. E.; Nkazi, D. B. Chemical modifications of castor oil: A review. *Sci. Prog.* 2019, *102*, 199–217.
- (25) Musik, M.; Bartkowiak, M.; Milchert, E. Advanced Methods for Hydroxylation of Vegetable Oils, Unsaturated Fatty Acids and Their Alkyl Esters. *Coatings* 2022, *12*, 13.
- (26) Chakraborty, I.; Chatterjee, K. Polymers and Composites Derived from Castor Oil as Sustainable Materials and Degradable Biomaterials: Current Status and Emerging Trends. *Biomacromolecules* 2020, 21, 4639–4662.
- (27) Meier, M. A. Plant-oil-based polyamides and polyurethanes: Toward sustainable nitrogen-containing thermoplastic materials. *Macromol. Rapid Commun.* 2019, *40*, 1800524.
- (28) Nekhavhambe, E.; Mukaya, H. E.; Nkazi, D. B. Development of castor oil-based polymers: A review. *J. Adv. Manuf. Process.* 2019, *1*, No. e10030.
- (29) Silva, J. A. C.; Grilo, L. M.; Gandini, A.; Lacerda, T. M. The Prospering of Macromolecular Materials Based on Plant Oils within the Blooming Field of Polymers from Renewable Resources. *Polymers* 2021, *13*, 1722.
- (30) Rist, M.; Greiner, A. Synthesis, Characterization, and the Potential for Closed Loop Recycling of Plant Oil-Based PA X.19 Polyamides. *ACS Sustain. Chem. Eng.* 2022, *10*, 16793–16802.
- (31) Patil, C. K.; Jung, D. W.; Jirimali, H. D.; Baik, J. H.; Gite, V. V.; Hong, S. C. Nonedible vegetable oil-based polyols in anticorrosive and antimicrobial polyurethane coatings. *Polymers* 2021, *13*, 3149.
- (32) Assefa, Y.; Purcell, L. C.; Salmeron, M.; Naeve, S.; Casteel, S. N.; Kovács, P.; Archontoulis, S.; Licht, M.; Below, F.; Kandel, H.; Lindsey, L. E.; et al. Assessing variation in US soybean seed composition (protein and oil). *Front. Plant Sci.* 2019, *10*, 298.
- (33) Kumar, V.; Vats, S.; Kumawat, S.; Bisht, A.; Bhatt, V.; Shivaraj, S. M.; Padalkar, G.; Goyal, V.; Zargar, S.; Gupta, S.; Kumawat, G.; et al. Omics advances and integrative approaches for the simultaneous improvement of seed oil and protein content in soybean (Glycine max L.). *Crit. Rev. Plant Sci.* 2021, *40*, 398–421.
- (34) Chen, C.; Cai, L.; Li, L.; Bao, L.; Lin, Z.; Wu, G. Heterogeneous and non-acid process for production of epoxidized soybean oil from soybean oil using hydrogen peroxide as clean oxidant over TS-1 catalysts. *Microporous Mesoporous Mater.* 2019, 276, 89–97.
- (35) He, W.; Zhu, G.; Gao, Y.; Wu, H.; Fang, Z.; Guo, K. Green plasticizers derived from epoxidized soybean oil for poly (vinyl chloride): Continuous synthesis and evaluation in PVC films. *Chem. Eng. J.* 2020, *380*, 122532.
- (36) Râpa, M.; Darie-Nita, R. N.; Matei, E.; Predescu, A. M. Bio-Based Plasticizers for Polyvinylchloride (PVC). Polyvinylchloride-Based Blends: Preparation. Characterization and Applications; Springer, 2022; pp 137–157..
- (37) Zilch, K. T., 2019, December. Industrial Uses of Soybean Oil. In *World Soybean Research Conference II*: CRC Press Proceedings 2019; pp 693–701.

- (38) Ribeiro, A. R.; Silva, S. S.; Reis, R. L. Challenges and opportunities on vegetable oils derived systems for biomedical applications. *Mater. Sci. Eng.* 2022, *134*, 112720.
- (39) Baghban, S. A.; Ebrahimi, M.; Khorasani, M. A facile method to synthesis of a highly acrylated epoxidized soybean oil with low viscosity: Combined experimental and computational approach. *Polym. Test.* 2022, *115*, 107727.
- (40) Mahdieh, A.; Motasadizadeh, H.; Yeganeh, H.; Nyström, B.; Dinarvand, R. Redox-responsive waterborne polyurethane nanocarriers for targeted doxorubicin delivery. *Int. J. Pharm.* 2022, 628, 122275
- (41) Yang, X.; Guo, M.; Wang, X.; Huan, W.; Li, M. Biobased Epoxies Derived from Myrcene and Plant Oil: Design and Properties of Their Cured Products. *ACS Omega* 2020, *5*, 28918–28928.
- (42) Intarabumrung, W.; Kuntharin, S.; Harnchana, V.; Prada, T.; Kasemsiri, P.; Hunt, A. J.; Supanchaiyamat, N. Facile Synthesis of Biobased Polyamide Derived from Epoxidized Soybean Oil as a High-Efficiency Triboelectric Nanogenerator. *ACS Sustainable Chem. Eng.* 2022, 10, 13680–13691.
- (43) Liu, Z.; Knetzer, D. A.; Wang, J.; Chu, F.; Lu, C.; Calvert, P. D. 3D printing acrylated epoxidized soybean oil reinforced with functionalized cellulose by UV curing. *J. Appl. Polym. Sci.* 2022, *139*, 51561.
- (44) Dąbrowska, A. Plant-Oil-Based Fibre Composites for Boat Hulls. *Materials* 2022, *15*, 1699.
- (45) Thomas, J.; Bouscher, R. F.; Nwosu, J.; Soucek, M. D. Sustainable Thermosets and Composites Based on the Epoxides of Norbornylized Seed Oils and Biomass Fillers. *ACS Sustainable Chem. Eng.* 2022, *10*, 12342–12354.
- (46) Gouda, K.; Bhowmik, S.; Das, B. A review on allotropes of carbon and natural filler-reinforced thermomechanical properties of upgraded epoxy hybrid composite. *Rev. Adv. Mater. Sci.* 2021, *60*, 237–275.
- (47) Armanasco, F.; D'hers, S.; Chiacchiarelli, L. M. Kinetic and chemorheological modeling of thermosetting polyurethanes obtained from an epoxidized soybean oil polyol crosslinked with glycerin. *J. Appl. Polym. Sci.* 2022, *139*, No. e53194.
- (48) Li, C.; Chen, Y.; Zeng, Y.; Wu, Y.; Liu, W.; Qiu, R. Strong and recyclable soybean oil-based epoxy adhesives based on dynamic borate. *Eur. Polym. J.* 2022, *162*, 110923.
- (49) Acar, M.; Çoban, S.; Hazer, B. Novel water soluble soya oil polymer from oxidized soya oil polymer and diethanol amine. *J. Macromol. Sci.*, Part A: Pure Appl. Chem. 2013, 50, 287–296.
- (50) Espinoza, S. M.; Patil, H. I.; San Martin Martinez, E.; Casañas Pimentel, R.; Ige, P. P. Poly-ε-caprolactone (PCL), a promising polymer for pharmaceutical and biomedical applications: Focus on nanomedicine in cancer. *Int. J. Polym. Mater. Polym. Biomater.* 2020, 69, 85–126.
- (51) Malik, S.; Subramanian, S.; Hussain, T.; Nazir, A.; Ramakrishna, S. Electrosprayed nanoparticles as drug delivery systems for biomedical applications. *Curr. Pharm. Des.* 2022, *28*, 368–379.
- (52) Li, Z.; Tan, B. H. Towards the development of polycaprolactone based amphiphilic block copolymers: molecular design, self-assembly and biomedical applications. *Mater. Sci. Eng. C* 2014, 45, 620–634.
- (53) Feng, P.; Wang, K.; Shuai, Y.; Peng, S.; Hu, Y.; Shuai, C. Hydroxyapatite nanoparticles in situ grown on carbon nanotube as a reinforcement for poly (ε-caprolactone) bone scaffold. *Mater. Today Adv.* 2022, *15*, 100272.
- (54) Inverardi, N.; Toselli, M.; Scalet, G.; Messori, M.; Auricchio, F.; Pandini, S. Stress-Free Two-Way Shape Memory Effect of Poly-(ethylene glycol)/Poly( $\epsilon$ -caprolactone) Semicrystalline Networks. *Macromolecules* 2022, *55*, 8533–8547.
- (55) Fan, C.; Huang, J.; Mensah, A.; Long, Z.; Sun, J.; Wei, Q. A high-performance and biodegradable tribopositive poly-ε-caprolactone/ethyl cellulose material. *Cell Rep. Phys. Sci.* 2022, *3*, 101012.
- (56) Madbouly, S.; Ougizawa, T. Binary miscible blends of poly(methyl methacrylate)/poly(α-methyl styrene-*co*-acrylonitrile):

- I. Rheological behavior. J. Macromol. Sci., Part B 2002, 41 (2), 255–269.
- (57) Urman, K.; Madbouly, S.; Otaigbe, J. U. Unusual accelerated molecular relaxations of a tin fluorophosphate glass/polyamide 6 hybrid studied by broadband dielectric spectroscopy. *Polymer* 2007, 48 (6), 1659–1666.
- (58) Mansour, A. A.; Madbouly, S. A. Dielectric investigation of the molecular dynamics of blends (II): polymers with dissimilar molecular architecture (PS/TMPC blend). *Polym. Int.* 1995, *37* (4), 267–276.
- (59) Mansour, A. A.; Madbouly, S. A. Dielectric investigation of the molecular dynamics in blends: polymers with similar molecular architecture (TMPC/PC blend). *Polym. Int.* 1995, *36* (3), 269–277.
- (60) Crivello, J. V.; Narayan, R. Epoxidized triglycerides as renewable monomers in photoinitiated cationic polymerization. *Chem. Mater.* 1992, *4*, 692–699.
- (61) Kumar, S.; Samal, S. K.; Mohanty, S.; Nayak, S. K. Epoxidized soybean oil-based epoxy blend cured with anhydride-based cross-linker: thermal and mechanical characterization. *Ind. Eng. Chem. Res.* 2017, *56* (3), 687–698.
- (62) Nepomuceno, N. C.; Fook, M. V. L.; Ries, A.; Mija, A.; Wellen, R. M. R. Bio-Based Epoxy Resins of Epoxidized Soybean oil Cured with Salicylic acid Loaded with Chitosan: Evaluation of Physical–Chemical Properties. *J. Polym. Environ.* 2023, *31* (6), 2566–2575.
- (63) Meng, Z.; He, J.; Cai, Z.; Wang, F.; Zhang, J.; Wang, L.; Ling, R.; Li, D. Design and additive manufacturing of flexible polycaprolactone scaffolds with highly-tunable mechanical properties for soft tissue engineering. *Mater. Des.* 2020, *189*, 108508.fuyrf.
- (64) Arbade, G. K.; Kumar, V.; Tripathi, V.; Menon, A.; Bose, S.; Patro, T. U. Emblica officinalis-loaded poly (ε-caprolactone) electrospun nanofiber scaffold as potential antibacterial and anticancer deployable patch. *New J. Chem.* 2019, *43* (19), 7427–7440.
- (65) De Graaf, L. A.; Beyer, J.; Möller, M. Spinodal phase separation in semi-interpenetrating polymer networks □ polystyrene-cross-polymethacrylate. *J. Polym. Sci. B Polym. Phys.* 1995, *33*, 1073−1084.
- (66) Shibita, A.; Takase, H.; Shibata, M. Semi-interpenetrating polymer networks composed of poly(l-lactide) and diisocyanate-bridged 4-arm star-shaped ε-caprolactone oligomers. *Polymer* 2014, 55, 5407–5416.
- (67) Rong, M.; Zeng, H. Polycarbonate-epoxy semi-interpenetrating polymer network: 2. Phase separation and morphology. *Polymer* 1997, 38, 269–277
- (68) Lipatov, Y. S.; Grigor'yeva, O. P.; Kovernik, G. P.; Shilov, V. V.; Sergeyeva, L. M. Kinetics and peculiarities of phase separation in the formation of semi-interpenetrating polymer network. *Die Makromolekulare Chem. Macromol. Chem. Phys.* 1985, *186*, 1401–1409.
- (69) Karabanova, L. V.; Boiteux, G.; Seytre, G.; Stevenson, I.; Lloyd, A. W.; Mikhalovsky, S. V.; Helias, M.; Sergeeva, L. M.; Lutsyk, E. D.; Svyatyna, A. Phase separation in the polyurethane/poly(2-hydroxyethyl methacrylate) semi-interpenetrating polymer networks synthesized by different ways. *Polym. Eng. Sci.* 2008, *48*, 588–597.
- (70) Jia, H.; Gu, S. Y.; Chang, K. 3D printed self-expandable vascular stents from biodegradable shape memory polymer. *Adv. Polym. Technol.* 2018, *37*, 3222–3228.
- (71) Morgan, R. A.; Loftus, I.; Ratnam, L.; Das, R.; Mailli, L.; Hamady, M. S.; Lobotesis, K. Clinical experience with a shape memory polymer peripheral vascular embolisation plug: a case series. *CVIR Endovasc.* 2021, *4*, 29.
- (72) Lendlein, A.; Langer, R. Biodegradable, elastic shape-memory polymers for potential biomedical applications. *Science* 2002, *296*, 1673–1676.
- (73) Li, G.; Fei, G.; Xia, H.; Han, J.; Zhao, Y. Spatial and temporal control of shape memory polymers and simultaneous drug release using high intensity focused ultrasound. *J. Mater. Chem.* 2012, *22*, 7692–7696.
- (74) Jana, S. Endothelialization of cardiovascular devices. *Acta Biomater*. 2019, *99*, 53–71.